Available online at www.sciencedirect.com
ScienceDirect
Trans. Nonferrous Met. Soc. China 30(2020) 417−427
Transactions of Nonferrous Metals Society of China
www.tnmsc.cn

Phase equilibria of Co−Mo−Zn ternary system

Zhi-yong PENG, Xin-ming WANG, Fu-cheng YIN, Xue-mei OUYANG, Jing-xian HU

Key Laboratory of Materials Design and Preparation Technology of Hunan Province, School of Materials Science and Engineering, Xiangtan University, Xiangtan 411105, China

Received 9 May 2019; accepted 17 September 2019

Abstract: To experimentally determine the isothermal sections of Co−Mo−Zn ternary system at 600 and 450 °C, the equilibrated alloy and diffusion couple methods were adopted by using scanning electron microscopy coupled with energy-dispersive spectrometry, X-ray diffractometry and electron probe microanalysis. Experimental results show that there are six three-phase regions on the Co−Mo−Zn isothermal section at 600 °C and nine three-phase regions on the Co−Mo−Zn isothermal section at 450 °C. No ternary compound is found in these two isothermal sections. Both the maximum solubilities of Mo in the Co−Zn compounds (γ-Co_5Zn_{21}, γ_1-$CoZn_7$, γ_2-$CoZn_{13}$ and β_1-CoZn) and that of Zn in ε-Co_3Mo are no more than 1.5 at.%. The maximum solubilities of Zn in μ-Co_7Mo_6 are determined to be 2.1 at.% and 2.7 at.% at 600 and 450 °C, respectively. In addition, the maximum solubilities of Co in $MoZn_7$ and $MoZn_{22}$ are 0.5 at.% and 4.7 at.% at 450 °C, respectively.

Key words: Co−Mo−Zn ternary system; phase diagram; solubility

1 Introduction

Hot dip galvanizing is one of the most cost-effective ways to improve the corrosion resistance of steel [1,2]. However, molten zinc bath is extremely corrosive to metallic materials [3−5]. As a result, the pot hardware, such as sink rolls, stabilizer rolls, and their bearings, are subjected to severe wear and corrosion during service periods. Frequent line stoppage for hardware replacement reduces production efficiency and increases zinc consumption, which causes huge losses.

Cobalt-based super-alloys are widely used for both sink rolls and stabilizer rolls in the galvanizing industry due to their relatively good resistance to wear and corrosion [6−9]. Molybdenum has a beneficial effect on the properties of cobalt-based alloys, improving their hardness, abrasion resistance and corrosion resistance [10,11]. Tribaloy series alloy (Co−Mo−Cr−Si alloy) is one of the representative cobalt-based alloys [12]. Its typical structure is a hard Laves phase + cobalt solid solution, in which Laves phase guarantees high strength and hardness, whereas cobalt matrix guarantees good toughness [13].

The development of the galvanized industrial materials such as Tribaloy series alloys has benefited from the systematic study of multi-phase relationship. However, the research on the phase relationship of the Co−Mo−Zn ternary system is still insufficient. The present work aimed to provide theoretical foundation for the development of wear-resistant and corrosion-resistant materials through experimentally determining the phase relationship of the Co−Mo−Zn ternary system including the isothermal sections at 600 and 450 °C.

Foundation item: Project (51771160) supported by the National Natural Science Foundation of China; Project (2018JJ4057) supported by the Scientific Research Fund of Hunan Provincial Science and Technology Department, China

Corresponding author: Xin-ming WANG; Tel: +86-731-58298428; E-mail: wangxm@xtu.edu.cn, fuchengyin@xtu.edu.cn

DOI: 10.1016/S1003-6326(20)65223-2

2 Literature data

Co−Mo−Zn ternary system consists of three binary phase diagrams, i.e. Co−Zn, Co−Mo, and Mo−Zn. The Co−Zn binary phase diagram has been investigated and summarized by HANSEN and ANDERKO [14] and MASSALSKI et al [15], which shows four intermediate phases in the Co−Zn system at 450 °C, namely, β_1-CoZn, γ-Co_5Zn_{21}, γ_1-$CoZn_7$, and γ_2-$CoZn_{13}$, respectively. The γ_2-$CoZn_{13}$ intermetallic compound does not exist at 600 °C. Recently, a thermodynamic description of the Co−Zn system has been carried out by ISOMÄKI and HÄMÄLÄINEN [16], VASSILEY and JIANG [17]. The main difference between them is that two intermetallic compounds, namely β-CoZn and δ-Co_2Zn_{15}, which have been experimentally confirmed [14,15], were omitted in the optimization work by ISOMÄKI and HÄMÄLÄINEN [16]. Experimental investigation and thermodynamic assessment of the Co−Mo binary system have been carried out by many scholars [18−24]. Lots of the data for the Co−Mo phase diagram have been calculated and assessed by BREWER and LAMOREAUX [25] who reported two intermetallic compounds in the Co−Mo system at 600 and 450 °C, viz., μ-Co_7Mo_6 and ε-Co_3Mo. Later, their findings were included in Refs. [15, 21]. DAVYDOV and KATTNER [22], DAVYDOV [23] and OIKAWA et al [24] sequentially evaluated and optimized Co−Mo binary system which agreed well with the finding of BREWER and LAMOREAUX [25]. Their results show that there is a slight difference in the temperature range of the existence of the σ phase and the solid solubility range of the μ phase. Compared with the Co−Zn and Co−Mo binary systems, the Mo−Zn system is relatively simple. The Mo−Zn binary phase diagram was originally calculated from a thermodynamic model based on data from MARTIN et al [26]. Using these results for thermodynamic modeling, BREWER and LAMOREAUX [25] calculated the total phase diagram in which two intermetallic compounds, $MoZn_7$ and $MoZn_{22}$, exist at 450 °C, but are not present at 600 °C. The results of the binary phase diagrams [15,25] were used in the present work, as shown in Fig. 1. And the crystallographic parameters for the binary compounds involved in Co−Mo−Zn system are listed in Table 1. Up to now, there is no information about the Co−Mo−Zn ternary phase diagram. Therefore, the phase equilibria of Co−Mo−Zn ternary system at 600 and 450 °C were investigated in this work.

3 Experimental

3.1 Equilibrated alloy preparation

The phase relationships of the Co–Mo–Zn ternary system at 600 and 450 °C were studied by using the equilibrated alloy. Each equilibrated alloy was prepared carefully using Zn powder, Co powder, and Mo powder, with the total mass of 3 g. The purity of all the starting materials was 99.99 wt.%. Due to its extremely high melting point, the dissolution and diffusion of Mo in the alloy mixtures were expected to be slow during the melting and homogenizing treatments. Hence, fine Mo powder used in this study was only 74 μm in size (200 mesh). The raw materials were mixed with appropriate amounts of each constituent and then sealed in evacuated quartz tube. Samples were slowly heated to 1200 °C and kept for 2 d, and

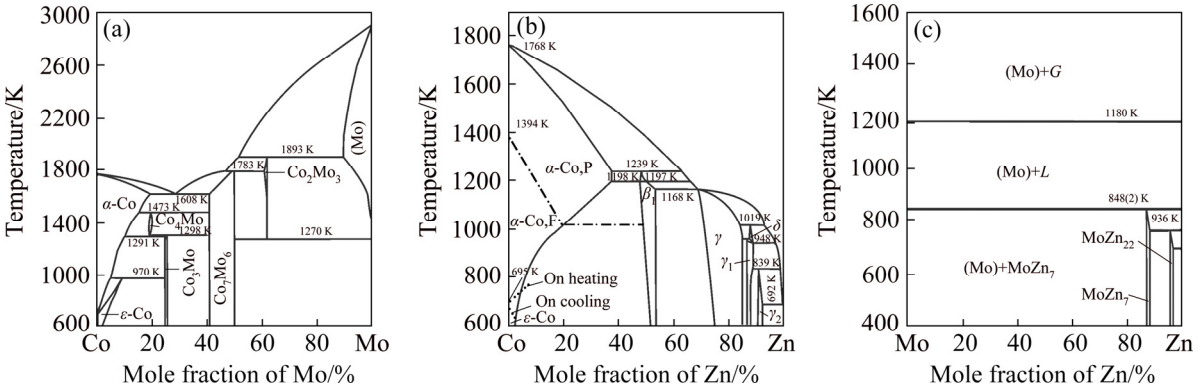

Fig. 1 Co−Mo [25] (a), Co−Zn [15] (b), and Mo−Zn [25] (c) binary phase diagrams adopted in this work

Table 1 Crystallographic parameters for binary compounds in Co−Mo−Zn system

Phase	Prototype	Pearson symbol	Space group	Lattice parameter/nm		
				a	*b*	*c*
β_1-CoZn	β-Mn	*cF*4	$P4_132$	0.6318	0.6318	0.6318
γ-Co_5Zn_{21}	Cu_5Zn_8	*cI*52	$I4_132$	0.8941	0.8941	0.8941
γ_1-$CoZn_7$	γ-brass related	*cF*16	*F*2/*m*	0.9030	0.4838	1.2511
γ_2-$CoZn_{13}$	$CoZn_{13}$	*mS*28	*C*2/*m*	1.3310	0.7535	0.4992
ε-Co_3Mo	Ni_3Sn	*hP*8	$P6_3/mmc$	0.5194	0.5194	0.4212
μ-Co_7Mo_6	Fe_7W_6	*hR*13	$R\bar{3}m$	0.4662	0.4662	2.5615
θ-Co_4Mo	Mg	*hP*2	$P6_3/mmc$	0.2597	0.2597	0.4212
σ-Co_2Mo_3	CrFe	*tP*30	$P4_2/mnm$	0.9228	0.9228	0.4826
$MoZn_7$	Ca_7Ge	−	−	0.7732	0.7732	0.7732
$MoZn_{22}$	−	−	−	0.6522	1.0654	0.9229
(Mo)	$CuAl_2$	*cI*2	$I4/mcm$	0.3147	0.3147	0.3147
η-Zn	Mg	*hP*2	$P6_3/mmc$	0.2664	0.2664	0.4946
ε-Co	Mg	*hP*2	$P6_3/mmc$	0.2507	0.2507	0.4068
α-Co	Cu	*cF*4	$Fm\bar{3}m$	0.3568	0.3568	0.3568

subsequently quenched in water using a bottom-quenching technique [27,28] which could effectively reduce Zn loss and sample porosity. The quenched samples were sealed again and annealed at 600 °C for 60 d and at 450 °C for 75 d, respectively, until an equilibrium state was reached. At last, all the samples were quenched in water rapidly to preserve the equilibrium state at annealing temperatures.

3.2 Diffusion couple preparation

Due to the higher liquidus temperatures of the Co-rich Co−Mo−Zn alloys, the diffusion couple method was employed to determine the phase relations at the Co-rich corner. The Co−Mo binary alloys including Co68.5Mo31.5, Co87.5Mo12.5, and Co90Mo10 were prepared by melting Co chips and Mo particles in an arc-furnace under high-purity argon atmosphere using a non-consumable tungsten electrode. The purities of the Co chips and Mo particles were 99.99 wt.%. Slices of approximate dimensions of 6 mm × 6 mm × 3 mm were cut from these Co−Mo binary alloy ingots. Each slice was ground, polished, cleaned, and then sealed together with 10 g zinc block in an evacuated quartz tube. The sealed specimens containing Co−Mo binary alloys Co68.5Mo31.5 and Co87.5Mo12.5 were annealed at 450 °C for 10 d while the sealed specimen containing alloy Co90Mo10 was annealed at 600 °C for 8 d, and then quenched into water.

3.3 Microstructure observation and phase compositions measurement

The samples were prepared in the conventional way for metallographic examinations. The 2 vol.% nital etching solution was used for revealing the microstructural details and a conventional optical microscope was used for the preliminary examination of all samples. The analyses of the morphology and the chemical composition of all phases in the equilibrated alloy samples were performed in a JSM−6360LV scanning electron microscope (SEM) equipped with OXFORD INCA energy-dispersive X-ray spectrometer (EDS). The constituent phase relations of the samples were further confirmed using X-ray diffraction patterns generated by a Rigaku Ultima IV X-ray diffractometer (Rigaku, Japanese), operating at 40 kV and 40 mA with Cu K_α radiation. The chemical compositions of the reaction zone in the diffusion couples were determined using EPMA (JEOL JXA−8230) operating at 15 kV. Pure Co, Mo, and Zn standard samples provided by JEOL were used for calibration.

4 Results and discussion

The phase relationships covering the entire composition range of the Co−Mo−Zn ternary system at 600 and 450 °C were studied by combining equilibrated alloy and diffusion couple

methods. The reported compositions are average values at least five measurements. The use of diffusion couples (DCs) in phase diagram studies is based on the principle of local equilibria at the phase interfaces in the diffusion region [29,30]. The compositions of three phases of each tie-triangle in the local equilibria obtained using EPMA from DC Co90Mo10/Zn at 600 °C and DC Co68.5Mo31.5/Zn and DC Co87.5Mo12.5/Zn at 450 °C. Based on the experimental results and phase diagram information of three sub-systems, the isothermal sections of Co−Mo−Zn system at 600 and 450 °C were constructed, as shown in Fig. 2. The detailed analysis of each isothermal section is listed as follows.

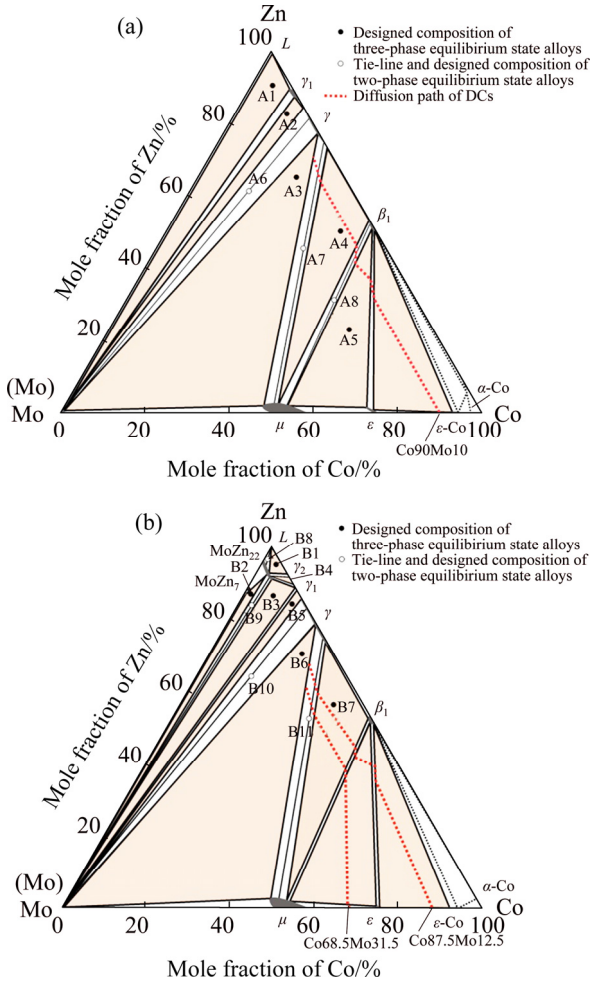

Fig. 2 Constructed isothermal sections of Co−Mo−Zn ternary system at different temperatures: (a) 600 °C; (b) 450 °C

4.1 Isothermal section of Co−Mo−Zn ternary system at 600 °C

A total of eight equilibrated alloys and one diffusion couple were used to determine the isothermal section of the Co−Mo−Zn system at 600 °C. Table 2 gives the designed compositions of alloys and phases in each equilibrated alloy, which were identified by a combination of XRD and SEM−EDS. Figure 2(a) shows the isothermal section of Co−Mo−Zn ternary system at 600 °C superimposed with nominal compositions of the alloys.

Table 2 Compositions of alloys and phases in Co−Mo−Zn ternary system at 600 °C

Alloy	Designed composition	Phase	Content/at.%		
			Co	Zn	Mo
A1	5Co−5Mo−90Zn	L	0.8	99.0	0.2
		γ_1	9.8	89.3	0.9
		(Mo)	0.6	0.3	99.1
A2	12Co−5Mo−83Zn	γ_1	11.9	87.2	0.9
		γ	15.6	84.0	0.4
		(Mo)	0.3	0.5	99.2
A3	23Co−12Mo−65Zn	μ	47.3	2.0	50.7
		(Mo)	0.6	0.7	98.7
		γ	22.6	77.2	0.2
A4	41Co−9Mo−50Zn	μ	50.6	2.1	47.3
		γ	26.8	73.0	0.2
		β_1	46.7	53.1	0.2
A5	57Co−20Mo−23Zn	μ	52.9	2.0	45.1
		β_1	48.5	51.0	0.5
		ε	72.0	1.5	26.5
A6	14Co−24Mo−62Zn	(Mo)	0.7	0.4	98.9
		γ	18.5	81.4	0.1
A7	35Co−20Mo−45Zn	μ	49.8	2.0	48.2
		γ	25.1	74.8	0.1
A8	49Co−20Mo−31Zn	μ	52.7	1.5	45.8
		β_1	47.4	52.2	0.4

The microstructure of Alloy A1 is shown in Fig. 3(a), in which the gray block γ_1 phase and white Mo-rich solid solution phase (Mo) are in equilibrium with the matrix of the porous liquid phase (marked as L in the present work). The XRD pattern, as shown in Fig. 3(b), also confirms the existence of these three phases. Figure 3(c) shows the three-phase equilibrium of (Mo), γ and γ_1. The white circular (Mo) phase and the light gray γ phase coexist with the matrix of the γ_1 phase. Also, they can be confirmed using the XRD pattern, as shown

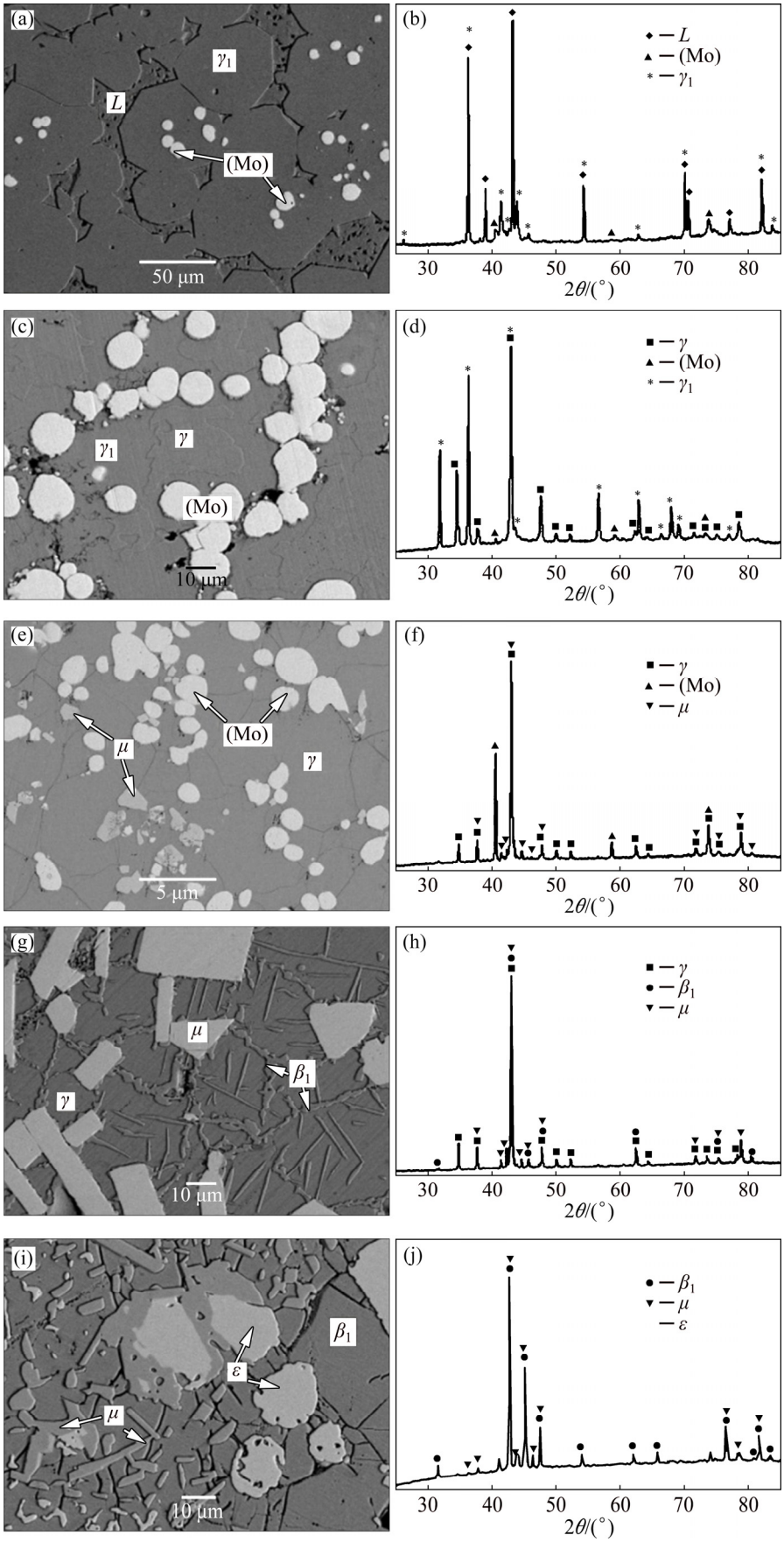

Fig. 3 Typical microstructures (a, c, e, g, i) and XRD patterns (b, d, f, h, j) corresponding to different three-phase fields of Alloys A1−A5 annealed at 600°C: (a, b) Alloy A1; (c, d) Alloy A2; (e, f) Alloy A3; (g, h) Alloy A4; (i, j) Alloy A5

in Fig. 3(d). SEM−EDS analyses indicated that Alloy A3 consists of three phases. The dark gray block is the μ phase, the light gray block is the (Mo) phase, and the matrix is the γ phase. The microstructure of this alloy is shown in Fig. 3(e) and the XRD pattern (Fig. 3(f)) clearly confirm the existence of μ, γ and (Mo) phases. Alloy A4 is in the μ+β_1+γ three-phase equilibrium state, as shown in Fig. 3(g). The light gray μ phase is uniformly distributed on the matrix γ phase, and the dark gray β_1 phase is grown in the dendritic form in the matrix γ phase. The XRD pattern of Alloy A4 is presented in Fig. 3(h). The microstructure of Alloy A5 obtained using SEM is shown in Fig. 3(i). SEM−EDS analyses suggest that Alloy A5 contains three phases, the dark gray μ phase, the light gray ε phase, and the matrix β_1 phase. The XRD pattern further confirms the result, as shown in Fig. 3(j).

By performing EPMA analysis, the valuable information about phase equilibria of Co–Mo–Zn ternary system at Co-rich corner and 600 °C was obtained. The microstructure of the DC Co90Mo10/Zn annealed at 600 °C for 8 d is shown in Fig. 4. It can be seen that the diffusion path close to the Co-rich corner of the DC Co90Mo10/Zn is ε-Co+ε→ε+β_1→β_1+μ→μ+γ. The compositions at the interfaces represent the tie-triangle data, as shown in Table 3. That means the DC Co90Mo10/Zn three-phase conjunction interfaces shown in Fig. 4 represent ε+ε-Co+β_1, β_1+ε+μ, and β_1+γ+μ three-phase equilibrium state.

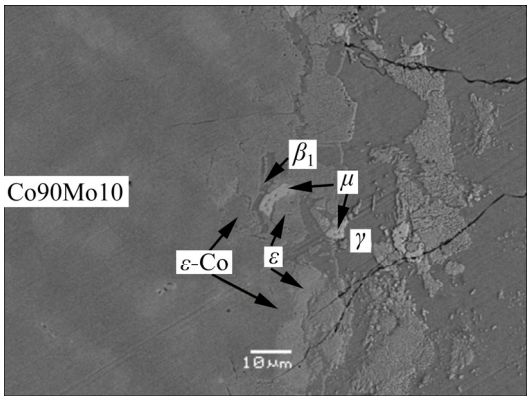

Fig. 4 Microstructure of DC Co90Mo10/Zn annealed at 600 °C for 8 d

Based on the present experimental results and combined with the results of binary phase diagram, the isothermal section of Co–Mo–Zn ternary system at 600 °C was constructed, as shown in Fig. 2(a), in which six three-phase regions are identified, viz. L+γ_1+(Mo), γ_1+γ+(Mo), μ+(Mo)+γ, μ+γ+β_1, μ+β_1+ε, and ε+ε-Co+β_1. The solubilities of Mo in the Co−Zn compounds (γ_1, γ, β_1) are very small, no more than 0.9 at.%, 0.4 at.%, and 0.5 at.%, respectively. The maximum solubilities of Zn in μ and ε are 2.1 at.% and 1.5 at.%, respectively. No ternary compound was observed.

Table 3 Tie-triangle data obtained with EMPA analyses for DC Co90Mo10/Zn at 600 °C

Tie-triangle	Phase	Content/at.%		
		Co	Zn	Mo
ε+ε-Co+β_1	ε-Co	92.88	0.21	6.91
	ε	73.84	0.92	25.24
	β_1	49.18	50.52	0.30
β_1+ε+μ	ε	72.14	1.22	26.64
	μ	52.57	2.06	45.37
	β_1	48.15	51.33	0.52
β_1+γ+μ	β_1	46.37	53.12	0.51
	γ	26.45	73.33	0.22
	μ	51.19	1.95	46.86

4.2 Phase equilibrium of Co−Mo−Zn ternary system at 450 °C

In order to investigate the phase relationship of Co−Mo−Zn system at 450 °C, eleven equilibrated alloys have been designed in this work, as shown in Table 4. Figure 2(b) shows the isothermal section of Co−Mo−Zn ternary system at 450 °C superimposed with the alloys' nominal compositions. According to the binary phase diagram data [15,25], the phase relationship of the Zn-rich corner at 450 °C is different from that at 600 °C due to the presence of γ_2-$CoZn_{13}$, $MoZn_7$ and $MoZn_{22}$. Therefore, in this section the phase equilibrium associated with γ_2-$CoZn_{13}$, $MoZn_7$ and $MoZn_{22}$ was focused on.

SEM−EDS analyses suggest that Alloy B1 contains three phases, i.e. L, γ_2 and $MoZn_{22}$. Fig. 5(a) shows the microstructure of Alloy B1. It can be easily differentiated by the morphology. The XRD pattern of this alloy further confirms the L+γ_2+ $MoZn_{22}$ three-phase equilibrated state, as shown in Fig. 5(b). A micrograph of Alloy B2 is shown in Fig. 5(c). This indicates that Alloy B2 consists of three phases, the white (Mo) phase, the light gray $MoZn_7$ phase, and the dark gray matrix

Table 4 Compositions of alloys and phases in Co−Mo−Zn ternary system at 450 °C

Alloy	Designed composition	Phase	Content/at.%		
			Co	Zn	Mo
B1	3Co−2Mo−95Zn	L	0.2	99.7	0.1
		$MoZn_{22}$	3.2	92.4	4.4
		γ_2	7.7	92.2	0.1
B2	2Co−12Mo−86Zn	$MoZn_7$	0.5	86.6	12.9
		$MoZn_{22}$	2.8	91.7	5.5
		(Mo)	0.3	0.3	99.4
B3	7Co−7Mo−86Zn	γ_1	11.5	88.4	0.1
		$MoZn_{22}$	4.7	90.8	4.5
		(Mo)	0.2	0.9	98.9
B4	8Co−2Mo−90Zn	γ_1	10.5	89.4	0.1
		γ_2	8.7	91.2	0.1
		$MoZn_{22}$	4.3	91.5	4.2
B5	13Co−4Mo−83Zn	γ	14.4	85.5	0.1
		(Mo)	0.6	0.9	98.5
		γ_1	12.1	87.8	0.1
B6	22Co−8Mo−70Zn	μ	48.5	2.7	48.8
		γ	21.1	78.8	0.1
		(Mo)	0.6	0.3	99.1
B7	36Co−8Mo−56Zn	μ	52.6	2.1	45.3
		γ	26.1	73.4	0.5
		β_1	46.7	52.4	0.9
B8	1Co−3Mo−96Zn	L	0.1	99.9	0
		$MoZn_{22}$	1.4	94.6	4.0
B9	4Co−12Mo−84Zn	$MoZn_{22}$	3.9	91.4	4.7
		(Mo)	0.1	0.8	99.1
B10	13Co−23Mo−64Zn	γ	16.9	82.7	0.4
		(Mo)	0.2	0.5	99.3
B11	32Co−15Mo−53Zn	μ	50.4	2.6	47.0
		γ	24.9	74.9	0.2

$MoZn_{22}$ phase. The XRD pattern of Alloy B2 is shown in Fig. 5(d). Figure 5(e) shows the microstructure of Alloy B3, and three phases are detected. The white (Mo) phase is distributed in the light gray $MoZn_{22}$ phase, and the dark gray matrix is γ_1 phase, which is further confirmed using XRD, as shown in Fig. 5(f). Alloy B4 corresponds to the $MoZn_{22}+\gamma_1+\gamma_2$ three-phase equilibrium state, as shown in Fig. 5(g), which is confirmed using XRD pattern, as shown in Fig. 5(h). Obviously, the light gray block phase is $MoZn_{22}$, while γ_1 and γ_2 can be distinguished by their microstructure.

The microstructures of Alloys B5, B6 and B7 are similar to that of Alloys A2, A3, and A4 at 600 °C, respectively. Alloy B5 contains three phases i.e. γ_1, (Mo) and γ. Alloy B6 is in μ+(Mo)+ γ three-phase equilibrium state. Alloy B7 consists of the μ phase, the γ matrix and the β_1 phase. The equilibrium microstructures of Alloys B5−B7 annealed at 450 °C are presented in Figs. 6(a−c), respectively.

Alloys B8 and B9 locate in two different $MoZn_{22}$-related two-phase regions, and the equilibrium microstructures of Alloys B8 and B9 are presented in Figs. 7(a) and (b), respectively. They contribute to constructing the solubility of the $MoZn_{22}$ phase. Figure 7(a) exhibits the microstructure of Alloy B8, which clearly shows two different phase regions. The light gray L phase is buried in the gray block which is considered to be the $MoZn_{22}$ phase with composition of Zn−1.4at.%Co−4.0at.%Mo. The equilibrium microstructure of Alloy B9 is presented in Fig. 7(b), indicating it locates in the (Mo) and $MoZn_{22}$ two-phase filed. The white phase is the solid solution phase (Mo), and the gray one is the $MoZn_{22}$ phase with composition of Zn−3.9at.%Co−4.7at.%Mo. Alloys B10 and B11 locate in two γ-related two-phase regions, which are similar in microstructure with Alloys A6 and A7 at 600 °C, as show in Figs. 7(c) and (d), respectively.

To further determine the phase relations of the Co−Mo−Zn ternary system at the Co-rich corner and 450 °C. Two diffusion couples, i.e. DC Co68.5Mo31.5/Zn and DC Co87.5Mo12.5/Zn, were prepared in the present work. Figure 8 illustrates the backscattered electron images of these two diffusion couples annealed at 450 °C for 10 d. The microstructures of the DC Co68.5Mo31.5/Zn are shown in Fig. 8(a). According to EPMA analysis, it can be known that the diffusion path close to the Co-rich corner of the DC Co68.5Mo31.5/Zn is $\varepsilon+\mu\rightarrow\mu+\beta_1\rightarrow\mu+\gamma$. There are $\beta_1+\varepsilon+\mu$ and $\beta_1+\gamma+\mu$ three-phase local equilibria at the conjunction interface in the diffusion zone. In addition, it can be seen from Fig. 8(b) that there are several local equilibrium regions (corresponding to different phases) at the DC Co87.5Mo12.5/Zn conjunction

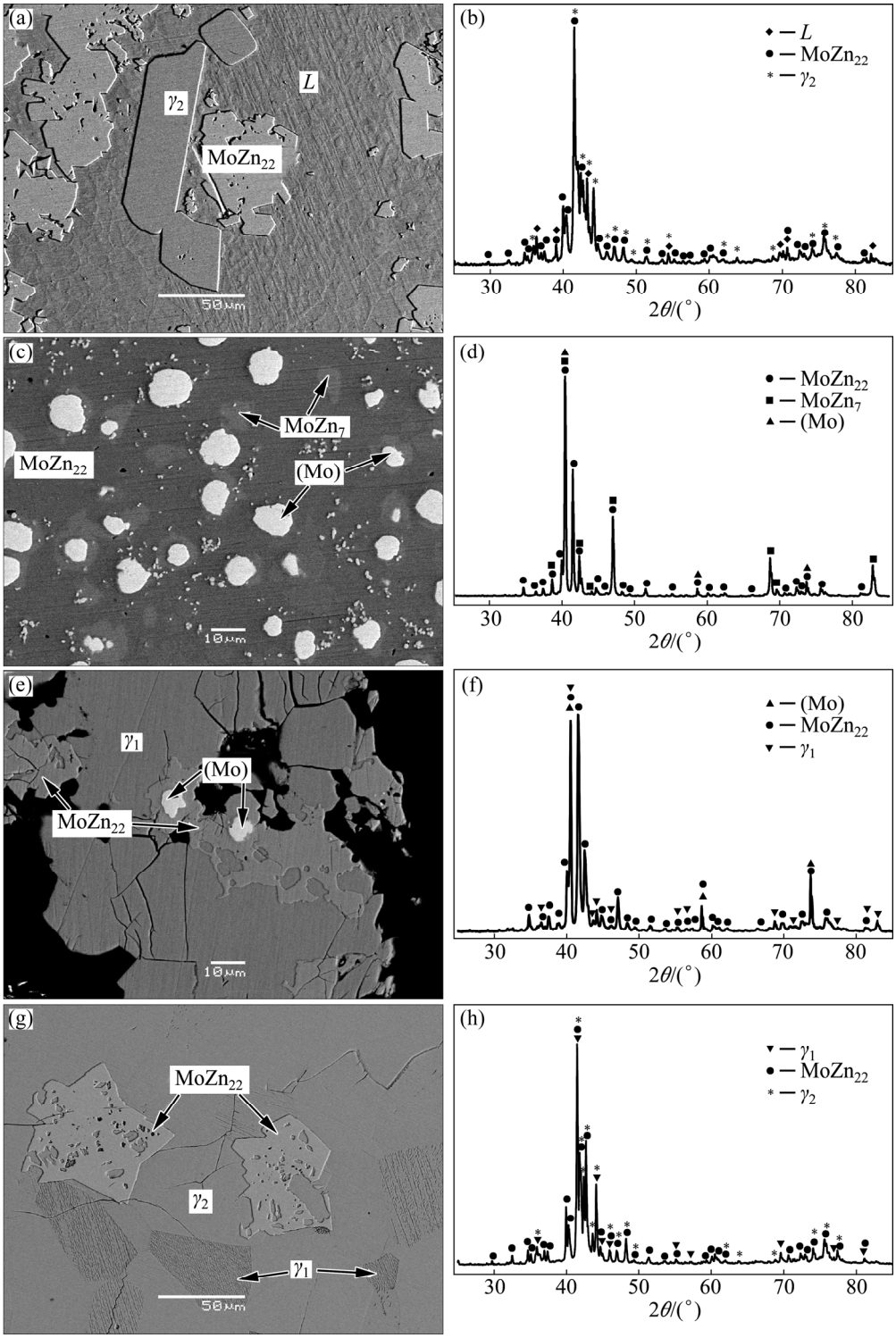

Fig. 5 Typical microstructures (a, c, e, g) and XRD patterns (b, d, f, h) corresponding to different three-phase fields of Alloys B1−B4 annealed at 450 °C: (a, b) Alloy B1; (c, d) Alloy B2; (e, f) Alloy B3; (g, h) Alloy B4

interface. By measuring the composition of phases near triple points, three three-phase fields can be obtained, including ε+ε-Co+β_1, β_1+ε+μ, and β_1+γ+μ. The diffusion path is induced as ε-Co+ε→ε+β_1→β_1+μ→μ+γ. As can be seen from Table 5, the compositions of the three phases in the same tie-triangle determined by different DCs are similar. The results verify the reliability of the diffusion couple method.

In summary, the isothermal sections of Co−Mo−Zn ternary system at 450 °C are constructed, as shown in Fig. 2(b). Nine three-phase regions were

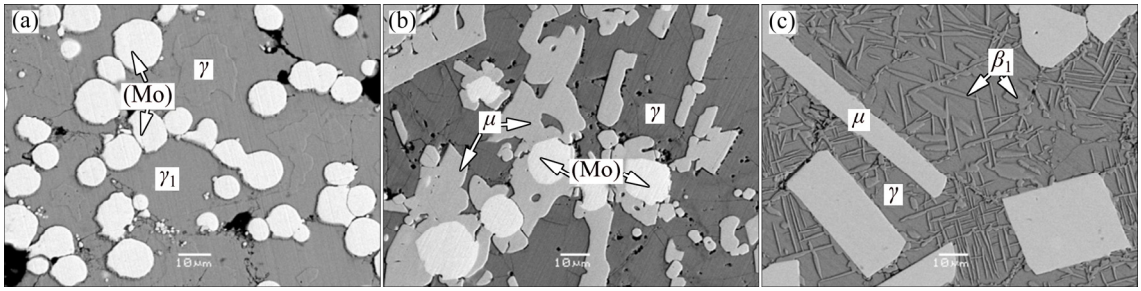

Fig. 6 Typical microstructures corresponding to different three-phase fields of Alloys B5−B7 annealed at 450 °C: (a) Alloy B5; (b) Alloy B6; (c) Alloy B7

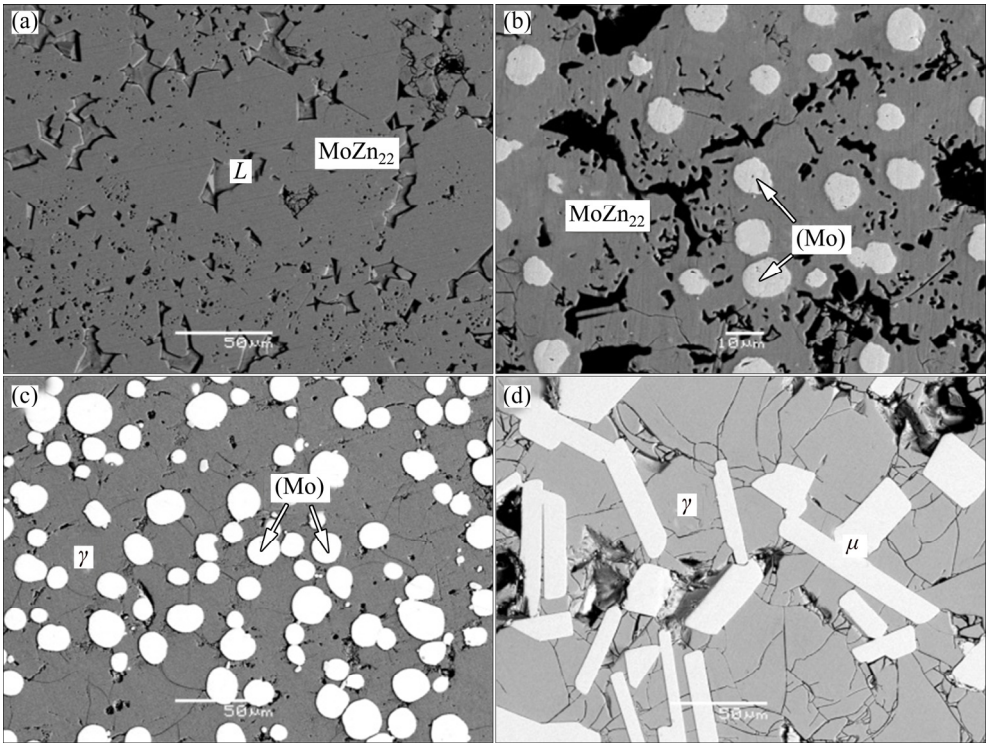

Fig. 7 Typical microstructures corresponding to different two-phase fields of Alloys B8−B11 annealed at 450 °C: (a) Alloy B8; (b) Alloy B9; (c) Alloy B10; (d) Alloy B11

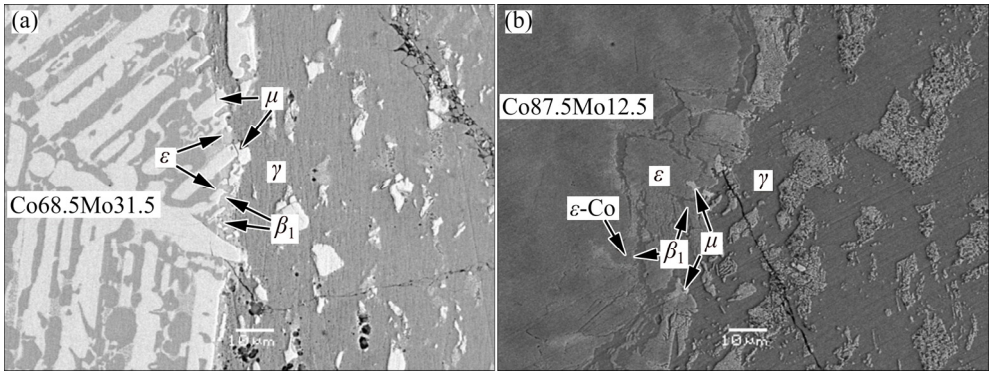

Fig. 8 Microstructures of different DCs annealed at 450 °C for 10 d: (a) Co68.5Mo31.5/Zn; (b) Co87.5Mo12.5/Zn

well established in the present work, viz. $L+\gamma_2+MoZn_{22}$, $MoZn_7+MoZn_{22}+$(Mo), γ_1+(Mo) $+MoZn_{22}$, $\gamma_1+\gamma_2+MoZn_{22}$, γ_1+(Mo)$+\gamma$, $\mu+$(Mo)$+\gamma$, $\mu+\gamma+\beta_1$, $\beta_1+\varepsilon+\mu$ and $\varepsilon+\varepsilon$-Co$+\beta_1$. Experimental results indicate that Mo is almost insoluble in γ_2 and γ_1, and the solid solubilities of Mo in γ and β_1 are also

limited, no more than 0.5 at.% and 0.9 at.%, respectively. The maximum solubilities of Co in $MoZn_7$ and $MoZn_{22}$ are 0.5 at.% and 4.7 at.%, respectively. The maximum solubilities of Zn in μ and ε are 2.7 at.% and 0.6 at.%, respectively. No ternary compound is found in this section.

Table 5 Tie-triangle data obtained with EMPA analyses for two DCs at 450 °C

Diffusion couple	Tie-triangle	Phase	Content/at.%		
			Co	Zn	Mo
Co68.5Mo31.5/Zn	$\varepsilon+\mu+\beta_1$	ε	74.55	0.64	24.81
		μ	53.43	1.92	44.65
		β_1	47.61	51.68	0.71
	$\beta_1+\gamma+\mu$	β_1	46.24	52.82	0.94
		γ	26.12	73.37	0.51
		μ	53.02	2.13	44.85
Co87.5Mo12.5/Zn	$\varepsilon+\varepsilon$-Co$+\beta_1$	ε-Co	92.23	0.15	7.62
		ε	75.58	0.14	24.28
		β_1	48.83	50.77	0.40
	$\varepsilon+\mu+\beta_1$	ε	74.36	0.59	25.05
		μ	53.29	1.88	44.83
		β_1	47.47	52.10	0.43
	$\beta_1+\gamma+\mu$	β_1	46.76	52.30	0.94
		γ	26.57	72.98	0.45
		μ	52.88	1.75	45.37

5 Conclusions

(1) Six three-phase regions, i.e. $L+\gamma_1$+(Mo), $\gamma_1+\gamma$+(Mo), μ+(Mo)+γ, $\mu+\gamma+\beta_1$, $\mu+\beta_1+\varepsilon$ and $\varepsilon+\varepsilon$-Co$+\beta_1$ have been identified experimentally in the Co−Mo−Zn ternary system at 600 °C.

(2) Nine three-phase regions, i.e. $L+\gamma_2+MoZn_{22}$, $MoZn_7+MoZn_{22}$+(Mo), γ_1+(Mo)+$MoZn_{22}$, $\gamma_1+\gamma_2+MoZn_{22}$, γ_1+(Mo)+γ, μ+(Mo)+γ, $\mu+\gamma+\beta_1$, $\beta_1+\varepsilon+\mu$ and $\varepsilon+\varepsilon$-Co$+\beta_1$ exist in the isothermal section at 450 °C.

(3) Both the maximum solubilities of Mo in the Co−Zn compounds (γ, γ_1, γ_2 and β_1) and that of Zn in ε-Co_3Mo are no more than 1.5 at.%. Furthermore, the maximum solubilities of Zn in μ-Co_7Mo_6 were determined to be 2.1 at.% and 2.7 at.% at 600 and 450 °C, respectively. In addition, the maximum solubilities of Co in $MoZn_7$ and $MoZn_{22}$ are 0.5 at.% and 4.7 at.% at 450 °C, respectively.

(4) No ternary compound is found in the two isothermal sections of the Co−Mo−Zn system at 600 and 450 °C.

References

[1] PISTOFIDIS N, VOURLIAS G, KONIDARIS S, PAVLIDOU E, STERGIOU A, STERGIOUDIS G. Microstructure of zinc hot-dip galvanized coatings used for corrosion protection [J]. Materials Letters, 2006, 60(6): 786−789.

[2] LI Z, SU X P, HE Y H, TAN Z, YIN F C. Growth of intermetallic compounds in solid Zn/Fe and Zn/Fe−Si diffusion couples [J]. Chinese Journal of Nonferrous Metals, 2008, 18(9): 1639−1644. (in Chinese)

[3] TOWNSEND H E, STEINBICKER R N, YAU Y H. Corrosion of stainless steel conductor rolls in a continuous sheet electrogalvanizing line [J]. Corrosion, 1990, 46(5): 418−423.

[4] MARDER A R. The metallurgy of zinc-coated steel [J]. Progress in Materials Science, 2000, 45(3): 191−271.

[5] ZHANG K, TANG N Y. Reactions of Co based and Fe based superalloys with a molten Zn−Al alloy [J]. Materials Science and Technology, 2004, 20(6): 739−746.

[6] PRZYBYLOWICZ J, KUSINSKII J. Laser cladding and erosive wear of Co−Mo−Cr−Si coatings [J]. Surface and Coatings Technology, 2000, 125(1): 13−18.

[7] ZHANG K, TANG N Y. On the wear of a cobalt-based superalloy in zinc baths [J]. Metallurgical and Materials Transactions A, 2003, 34(10): 2387−2396.

[8] ZHANG K. Wear of cobalt-based alloys sliding in molten zinc [J]. Wear, 2003, 255(1): 545−555.

[9] YE P, YIN F C, LIU Y, OUYANG X M, XIE X L. Corrosion resistance of liquid zinc of FeB/Co cermet coating deposited by AC-HVAF [J]. Chinese Journal of Nonferrous Metals, 2018, 28(4): 782−791. (in Chinese)

[10] SZCZYGIEL B, LASZCZYŃSKA A, TYLUS W. Influence of molybdenum on properties of Zn−Ni and Zn−Co alloy coatings [J]. Surface and Coatings Technology, 2010, 204(9): 1438−1444.

[11] JIANG S L. Phase equilibrium of the Co−Mo−Cr−Si quaternary system and corrosion resistance in molten zinc bath [D]. Xiangtan: Xiangtan University, 2014: 39−47. (in Chinese)

[12] YAO M X, WU J B C, YICK S, XIE Y, LIU R. High temperature wear and corrosion resistance of a Laves phase strengthened Co−Mo−Cr−Si alloy [J]. Materials Science and Engineering A, 2006, 435(3): 78−83.

[13] LIU Y X, CHEN X, YIN F C, OU L F, LI Z, ZHAO M X. Microstructure and corrosion resistance in liquid Al bath of Co−Mo−Cr−Si alloys [J]. Chinese Journal of Nonferrous Metals, 2018, 28(10): 2033−2042. (in Chinese)

[14] HANSEN M, ANDERKO K. Constitution of binary alloys [J]. Journal of the Electrochemical Society, 1958, 105(12): 260C−261C.

[15] MASSALSKI T B, OKAMOTO H, SUBRAMANIAN P R, AND KACPRZAK L. Binary alloy phase diagrams [M]. 2nd ed. Ohio: ASM International, 1990.
[16] ISOMÄKI I, HÄMÄLÄINEN M. Thermodynamic evaluation of the Co−Zn system [J]. Journal of Alloys and Compounds, 2004, 375(1−2): 191−195.
[17] VASSILEY G P, JIANG M. Thermodynamic optimization of the Co−Zn system [J]. Journal of Phase Equilibria and Diffusion, 2004, 25(3): 259−268.
[18] QUINN T J, HUME-ROTHERY W. The equilibrium diagram of the system molybdenum−cobalt [J]. Journal of the Less Common Metals, 1963, 5(4): 314−324.
[19] HEIJWEGEN C P, RIECK G D. Determination of the phase diagram of the Mo−Co system using diffusion couples [J]. Journal of the Less Common Metals, 1974, 34(2): 310−314.
[20] GUST W, PREDEL B, MEHRA S N. Kinetics of finely lamellar discontinuous precipitation in Co−Mo mixed crystals [J]. Materials Science and Engineering A, 1975, 21(2): 131−138.
[21] OKAMOTO H. Desk handbook-phase diagrams for binary alloys [M]. Ohio: ASM International, 2000.
[22] DAVYDOV A, KATTNER U R. Thermodynamic assessment of the Co−Mo system [J]. Journal of Phase Equilibria and Diffusion, 1999, 20(1): 5−16.
[23] DAVYDOV A. Revised thermodynamic description for the Co−Mo system [J]. Journal of Phase Equilibria and Diffusion, 2003, 24(3): 209−211.
[24] OIKAWA K, KATTNER U R, SATO J, OMORI T, JIANG M, ANZAI K, ISHIDA K. Experimental determination and thermodynamic assessment of phase equilibria in the Co−Mo System [J]. Materials Transactions, 2012, 53: 1425−1435.
[25] BREWER L, LAMOREAUX R H. Molybdenum: Physico−chemical properties of its compounds and alloys [M]. Vienna: International Atomic Energy Agency, 1980.
[26] MARTIN A E, KNIGHTON J B, FEDER H M. Solubilities in liquid zinc, zirconium, niobium, molybdenum, palladium, and thorium [J]. Journal of Chemical and Engineering Data, 1961, 6(4): 596−599.
[27] LIU Y X, YIN F C, LI Z, OUYANG X M, CHEN L P. Experimental determination of 800 °C isothermal section in Al−Zn−Zr ternary system [J]. Transactions of Nonferrous Metals Society of China, 2019, 29(1): 25−33.
[28] LIU Y X, YIN F C, HU J X, LI Z, CHENG S H. Phase equilibria of Al−Fe−Sn ternary system [J]. Transactions of Nonferrous Metals Society of China, 2018, 28(2): 282−289.
[29] WANG M, LIU H S, CAI G M, JIN Z P. Measurement of phase equilibria in Ti−Ni−Sn system [J]. Transactions of Nonferrous Metals Society of China, 2018, 28(4): 819−828.
[30] GUO Z K, LIN Z X, YAN D S. High temperature phase equilibria and phase diagrams [M]. Shanghai: Shanghai Scientific and Technical Publishers, 1987. (in Chinese)

Co−Mo−Zn 三元体系的相平衡

彭志勇，王鑫铭，尹付成，欧阳雪枚，胡静娴

湘潭大学 材料科学与工程学院 材料设计及制备技术湖南省重点实验室，湘潭 411105

摘 要：采用平衡合金法和扩散偶法，通过扫描电子显微镜结合能量色散光谱、X 射线衍射和电子探针微量分析，实验测定 Co−Mo−Zn 三元体系在 600 和 450 °C 的等温截面。实验结果表明，对于所构建的 Co−Mo−Zn 三元体系，600 °C 等温截面中存在 6 个三相区，450 °C 等温截面中存在 9 个三相区，在此两个等温截面中未发现三元化合物。Mo 在 Co−Zn 化合物(γ-Co_5Zn_{21}，γ_1-$CoZn_7$，γ_2-$CoZn_{13}$ 和 β_1-CoZn)中的最大溶解度和 Zn 在 ε-Co_3Mo 中的最大溶解度均不大于 1.5 at.%。600 和 450 °C 时，Zn 在 μ-Co_7Mo_6 中的最大溶解度分别为 2.1 at.%和 2.7 at.%。此外，450 °C 时，Co 在 $MoZn_7$ 和 $MoZn_{22}$ 中的最大溶解度分别为 0.5 at.%和 4.7 at.%。

关键词：Co−Mo−Zn 三元体系；相图；固溶度

(Edited by Wei-ping CHEN)